

1 Supplement

2 S1. Landslide runout modelling using DAN3D-Flex

3 Landslide runout has been modelled in recent years by multiple authors (Allen et al., 2009; Grämiger et al., 2016;
4 Hungr and Evans, 1996; Nagelisen et al., 2015; Preuth et al., 2010; Sosio et al., 2008; Xing et al., 2015) and
5 different software programs are available. One of them is Dynamic Analysis 3D (DAN3D) presented by
6 McDougall & Hungr (2004). In DAN3D, a frictional model defines material behaviour using the meshless
7 Lagrangian numerical technique known as "smoothed particle hydrodynamics" (SPH). The modeller may choose
8 between frictional, plastic, Bingham, Newtonian, and Voellmy rheology. McDougall & Hungr (2004) found that
9 landslide behaviour is best reconstructed when using frictional or Voellmy basal rheology. Frictional rheology is
10 characterised by Eq. (1), where τ is the basal shear stress, σ_z the bed normal stress and φ_b is the bulk friction
11 angle. The Voellmy rheology is defined by Eq. (2), where μ is the frictional coefficient (equivalent to $\tan \varphi_b$), ρ
12 is the material density in kg m^{-3} , g the gravitational acceleration in m s^{-2} , v is the depth-averaged flow velocity in
13 m s^{-1} , and ξ is the turbulence coefficient in m s^{-2} .

$$14 \quad \tau = \sigma_z \tan \varphi_b \quad (1)$$

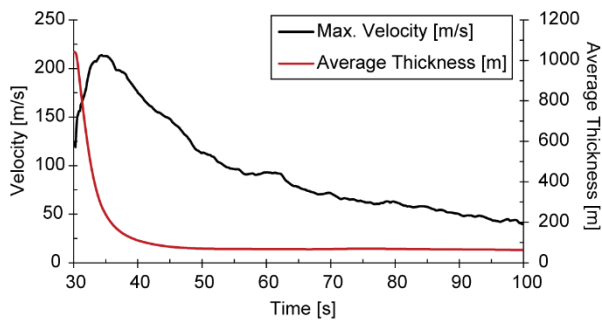
$$15 \quad \tau = \sigma_z \mu + \frac{\rho g v^2}{\xi} \quad (2)$$

16 The input parameters for both rheologies need to be defined through back-analysis. Constraints on the parameters
17 may be deduced from the deposit's extent, the runout topography, and the material exposed along the sliding path.
18 Additionally, previous studies provide first estimates of reasonable input parameters in similar environments. A
19 common issue when modelling with DAN3D is that fluid pressure induces lateral spreading of a flow-like rock
20 mass already in the source area (Aaron and Hungr, 2016b). However, it is more reasonable to assume the rock
21 mass slides without much internal deformation in the rock avalanche's early stages. Therefore, a modified dynamic
22 model was developed by Aaron et al. (2017), which allows for the simulation of an initial coherent phase of motion
23 followed by the flow-like movement of a rock avalanche (DAN3D-Flex). The modified dynamic model results
24 in a more accurate representation of rock slope failures (Aaron et al., 2017), and was used in this study.

25 DAN3D-Flex is the follow-up dynamic runout modelling program to DAN3D. It is used to model the runout of
26 rapid mass movements across three-dimensional input topographies. The required input parameters are
27 determined using back-analysis and include the internal friction of the material (φ_i) and the basal rheology
28 (frictional and Voellmy) and their respective controlling parameters. If the frictional rheology is applied, a
29 definition of basal friction (φ_b) and relative pore pressure (ru) is required. When applying the Voellmy model,
30 the friction coefficient μ and the turbulence coefficient ξ need to be defined. For rock avalanches, frictional or
31 Voellmy rheology should be used (Aaron and Hungr, 2016b; Hungr, 1995). Many authors successfully applied
32 either one of these rheologies (Grämiger et al., 2016; Nagelisen et al., 2015), but Aaron and Hungr (Aaron and
33 Hungr, 2016a) argue that while initial displacement is better simulated in frictional rheology, Voellmy rheology
34 approximates the runout in the deposition area better as it becomes more fluid-like. Runout modelling delivers
35 information on the travel path, movement parameters, and deposit thickness and extent.

36 **S2. Caveats on the landslide runout modelling**

37 We are confident that the runout modelling approximates a realistic landslide, mainly because the results are
38 consistent with our field observations. However, we here discuss three significant limitations to the model. Firstly,
39 the runout velocity reached a brief maximum of $\sim 200 \text{ m s}^{-1}$ (Fig. S1), which is a staggeringly high value,
40 considering that published reports from historical and modern rock avalanches report maximum velocities of \sim
41 150 km h^{-1} (Scheidegger, 1973; Sosio et al., 2008; USGS, 2016). Even though internal mechanisms such as rock
42 fragmentation may reduce frictional resistance on the sliding surface, thus increasing runout speed (Davies and
43 McSaveney, 2009; McSaveney and Davies, 2006), and the sand cloud resulting from the impact of the rock slab
44 with the valley floor will have travelled faster than the ground-based landslide, it remains unlikely that the initial
45 landslide reached runout velocities of 200 m s^{-1} . Secondly, the deposit's thickness right after impact is reported as
46 1040 m , which is likely an overestimation (Fig. S1). The model does not differentiate between the rockfall on the
47 ground and what we call the dust cloud. It remains unclear whether the fine particles reached such an elevation,
48 but it appears a possible option. Finally, we ran only a small number of models. Nevertheless, within these model
49 runs, we managed to implement several parameter combinations, and at least one resulted in a realistic landslide
50 runout. Thus, the feasibility of the proposed processes was tested successfully, and we achieved the primary goal
51 of runout modelling.



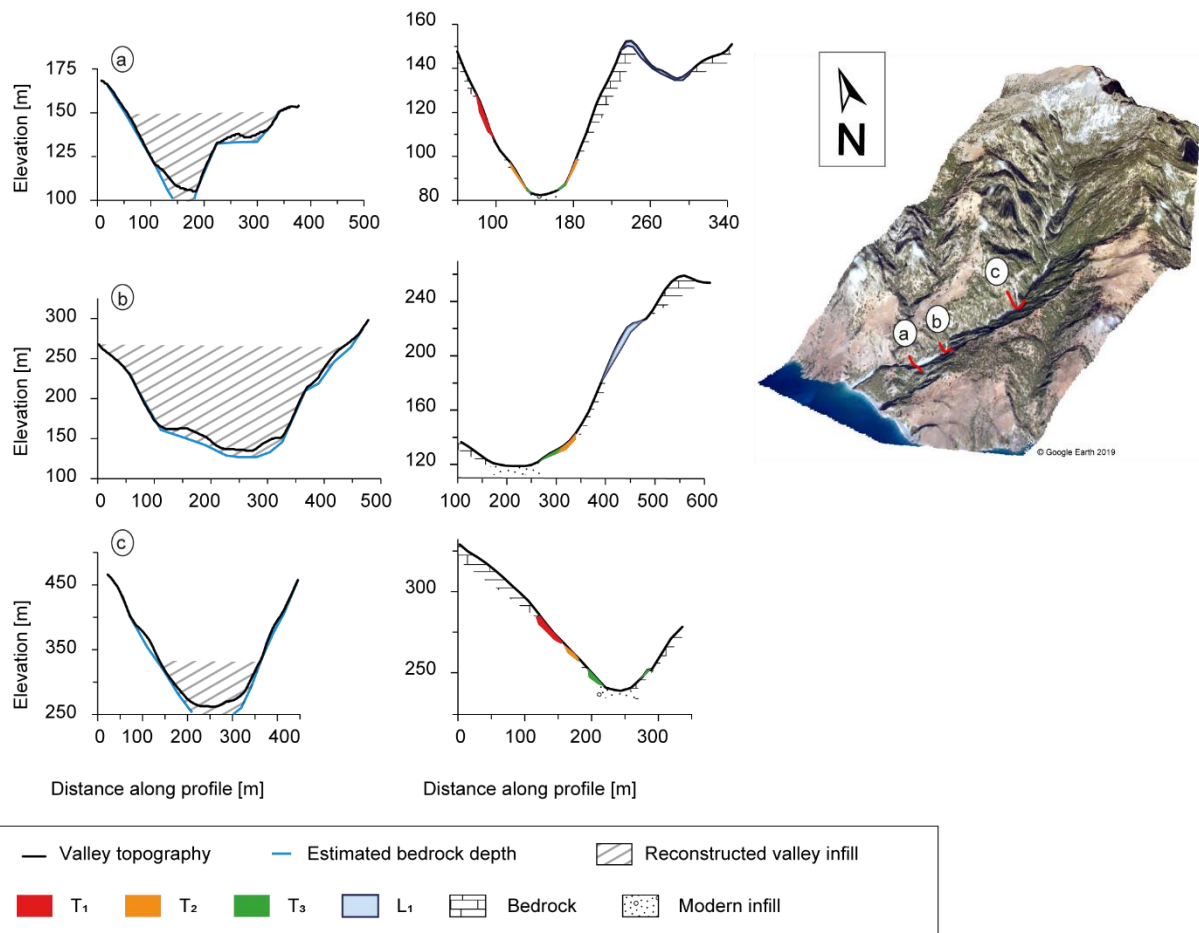
52

53 **Figure S1:** Dan3D-Flex output from the best-fit runout model.

54 **S3. Estimating valley bedrock topography for landslide runout modelling**

55 The initial landslide filled a sediment-limited valley, with a stream that incised the bedrock, with large amounts
 56 of unconsolidated sediment. Thus, to guarantee a representative flow surface for the landslide runout modelling,
 57 it was necessary to approximate these conditions by "removing" the Holocene deposits. For the calculation, we
 58 assumed that the Holocene deposits are of constant thickness throughout the valley, with their upper depositional
 59 surfaces minimally modified by post-depositional processes (e.g. subsequent erosion). ArcMap 10.2 was used for
 60 calculations.

61 Twenty-six topographic profiles, up to 1,200 m in length, were constructed across the valley's width (Fig. S2).
 62 The profiles were assigned elevation values from a 5 m DEM that were then exported to an attribute table and an
 63 imaging program. Using our detailed field observations and reports by Booth (2010), we visually marked the
 64 landslide locations and alluvial infill deposits on these profiles. Subsequently, the deposit thicknesses were
 65 subtracted from the modern topography, resulting in an estimate of the valley's pre-landslide bedrock topography
 66 (DEMpre).



67
 68 **Figure S2:** Left panel: Exemplary valley profiles of modern topography (black curve), whose location is highlighted in the 3D
 69 imagery (red) produced using ArcScene 10.6.1 (ESRI, 2011). The blue curve is assumed bedrock depth as calculated from
 70 subtracting the thickness of each Holocene infill deposit from the modern topography (DEMpre). The striped shading
 71 represents the assumed landslide infill based on field mapping and volume calculations. The process was repeated for 26
 72 profiles across the river, and the results were implemented to produce DEMpre. Right panel: Mapping of the Holocene deposits
 73 at the location of each profile. The thicknesses are not representative.

74 **S4. Radiocarbon measurement detailed report**

75 **Table S5:** Detailed report of bulk sediment radiocarbon measurements. All measurements were conducted at the Laboratory
 76 of Ion Beam Physics, ETH Zürich.

ETH number	Label	Description	C (µg)	Fm	Error absolute	Fm corrected	Error	¹⁴ C ages (yrs, 1 σ)	Error (yrs)
94494.1.1	4	Tributary deposit 1	37	0.5729	0.00690	0.55	0.04	4820	556
87102.1.1	4	Tributary deposit 1	41	0.7111	0.00694	0.71	0.03	2696	369
94495.1.1	5	Tributary deposit 2	52	0.5660	0.00690	0.55	0.03	4820	379
87100.1.1	5	Tributary deposit 2	30	0.6630	0.00657	0.66	0.05	3389	587
94493.1.1	6	Lower fan	27	0.5832	0.00680	0.55	0.05	4793	826
94491.1.1	7	Upper fan 1	29	0.5309	0.00650	0.49	0.05	5788	874
87099.1.1	7	Upper fan 1	24	0.6128	0.00714	0.59	0.06	4304	903
87103.1.1	8	Upper fan 2	20	0.5792	0.00602	0.53	0.08	5131	1342
94496.1.1	9	Landslide deposit	42	0.7280	0.00740	0.73	0.03	2476	351
87098.1.1	9	Landslide deposit	23	0.6709	0.00737	0.66	0.07	3294	831

77

78 S5. Overview of infill deposits in the valley



79

80 **Figure S3:** Full-valley mapping of sedimentary deposits and landslide deposits. All deposits are distributed along the valley's
81 entire length, suggesting a shared place of origin in the headwaters. For more mapping details of the terrace and fan deposits,
82 see Booth (2010).

83 **S6. References**

- 84 Aaron, J. and Hungr, O.: Dynamic analysis of an extraordinarily mobile rock avalanche in the Northwest
85 Territories, Canada, *Can. Geotech. J.*, 53(6), 899–908, doi:10.1139/cgj-2015-0371, 2016a.
- 86 Aaron, J. and Hungr, O.: Dynamic simulation of the motion of partially-coherent landslides, *Eng. Geol.*, 205, 1–
87 11, doi:10.1016/j.enggeo.2016.02.006, 2016b.
- 88 Aaron, J., McDougall, S., Moore, J. R., Coe, J. A. and Hungr, O.: The role of initial coherence and path
89 materials in the dynamics of three rock avalanche case histories, *Geoenvironmental Disasters*, 4(1), 5,
90 doi:10.1186/s40677-017-0070-4, 2017.
- 91 Allen, S. K., Schneider, D. and Owens, I. F.: First approaches towards modelling glacial hazards in the Mount
92 Cook region of New Zealand's Southern Alps, *Nat. Hazards Earth Syst. Sci.*, 9(2), 481–499, doi:10.5194/nhess-
93 9-481-2009, 2009.
- 94 Booth, J.: The response of Mediterranean steep-land coastal catchments to base level and climate change,
95 southwestern Crete, Aberystwyth University., 2010.
- 96 Davies, T. R. and McSaveney, M. J.: The role of rock fragmentation in the motion of large landslides, *Eng.*
97 *Geol.*, 109(1–2), 67–79, doi:10.1016/j.enggeo.2008.11.004, 2009.
- 98 ESRI: National Geographic World Map, digital topographic basemap of the world., *Natl. Geogr. Esri, DeLorme,*
99 *NAVTEQ, UNEP-WCMC, USGS, NASA, ESA, METI, NRCAN, GEBCO, NOAA, IPC* [online] Available
100 from: <https://www.arcgis.com/home/item.html?id=b9b1b422198944fbbd5250b3241691b6#overview> (Accessed
101 21 September 2017), 2011.
- 102 Grämiger, L. M., Moore, J. R., Vockenhuber, C., Aaron, J., Hajdas, I. and Ivy-Ochs, S.: Two early Holocene
103 rock avalanches in the Bernese Alps (Rinderhorn, Switzerland), *Geomorphology*, 268, 207–221,
104 doi:10.1016/j.geomorph.2016.06.008, 2016.
- 105 Hungr, O.: A model for the runout analysis of rapid flow slides, debris flows, and avalanches, *Can. Geotech. J.*,
106 32(4), 610–623, doi:10.1139/t95-063, 1995.
- 107 Hungr, O. and Evans, S. G.: Rock avalanche runout prediction using a dynamic model, *Proc. 7th Int. Symp.*
108 *Landslides, Trondheim, Norw.*, 17, 21 [online] Available from: <http://www.clara-w.com/DANWReference2.pdf>,
109 1996.
- 110 McDougall, S. and Hungr, O.: A model for the analysis of rapid landslide motion across three-dimensional
111 terrain, *Can. Geotech. J.*, 41, 1084–1097, doi:10.1139/T04-052, 2004.
- 112 McSaveney, M. J. and Davies, T. R.: Inferences from the morphology and internal structure of rockslides and
113 rock avalanches rapid rock mass flow with dynamic fragmentation, in *Landslides from Massive Rock Slope*
114 *Failure*, edited by S. G. Evans, G. S. Mugnozza, A. Strom, and R. L. Hermanns, Springer, Dordrecht., 2006.
- 115 Nagelisen, J., Moore, J. R., Vockenhuber, C. and Ivy-Ochs, S.: Post-glacial rock avalanches in the Obersee
116 Valley, Glarner Alps, Switzerland, *Geomorphology*, 238, 94–111, doi:10.1016/j.geomorph.2015.02.031, 2015.
- 117 Preuth, T., Bartelt, P., Korup, O. and Mc Ardell, B. W.: A random kinetic energy model for rock avalanches:
118 Eight case studies, *J. Geophys. Res. Earth Surf.*, 115(3), F03036, doi:10.1029/2009JF001640, 2010.
- 119 Scheidegger, A. E.: On the prediction of the reach and velocity of catastrophic landslides, *Rock Mech.*
120 *Felsmechanik Mécanique des Roches*, 5(4), 231–236, doi:10.1007/BF01301796, 1973.
- 121 Sosio, R., Crosta, G. B. and Hungr, O.: Complete dynamic modeling calibration for the Thurwieser rock
122 avalanche (Italian Central Alps), *Eng. Geol.*, 100(1–2), 11–26, doi:10.1016/j.enggeo.2008.02.012, 2008.
- 123 USGS: Catastrophic Landslides of the 20th Century - Worldwide, USGS - Landslide Hazards [online] Available
124 from: [https://www.usgs.gov/natural-hazards/landslide-hazards/science/catastrophic-landslides-20th-century-
125 worldwide?qt-science_center_objects=0#qt-science_center_objects](https://www.usgs.gov/natural-hazards/landslide-hazards/science/catastrophic-landslides-20th-century-worldwide?qt-science_center_objects=0#qt-science_center_objects) (Accessed 20 July 2018), 2016.
- 126 Xing, A. G., Xu, Q. and Gan, J. J.: On characteristics and dynamic analysis of the Niumian valley rock
127 avalanche triggered by the 2008 Wenchuan earthquake, Sichuan, China, *Environ. Earth Sci.*, 73(7), 3387–3401,
128 doi:10.1007/s12665-014-3626-6, 2015.

129